Int J Adv Manuf Technol (2016) 83:347–355
DOI 10.1007/s00170-015-7567-3

ORIGINAL ARTICLE

A model for prediction of subsurface damage in rotary ultrasonic face milling of optical K9 glass

Jianjian Wang[1,3] · **Chenglong Zhang**[2] · **Pingfa Feng**[1,3] · **Jianfu Zhang**[1,3]

Received: 7 March 2015 / Accepted: 5 July 2015 / Published online: 24 July 2015

Abstract Subsurface damage (SSD) induced by the rotary ultrasonic face machining (RUFM) considerably influences the technological application of the optical components. However, currently, there is no method to detect the depth of SSD in real time. For the purpose of precise and nondestructive evaluation of the SSD depth generated in RUFM processes, a predictive model was developed by applying the indentation fracture mechanics of brittle material. This was the first time that the correlation between the measured cutting force and SSD depth had been established. It was found that the SSD depth was directly proportional to the exponent of the measured cutting force (namely $d_{SSD}=\gamma F_c^{\chi}$). Using this model, the depth of SSD could be predicted rapidly and precisely in the RUFM of optical glass even in real time using the measuring cutting force. Subsequently, this method was verified by conducting RUFM tests on K9 glass specimens with Sauer Ultrasonic 50. Meanwhile, the cutting force and SSD depth were compared experimentally between RUFM and conventional grinding (CG) process, indicating that RUFM is a beneficial manufacturing method for optical glass with reduced cutting force and SSD depth.

✉ Pingfa Feng
fengpf@mail.tsinghua.edu.cn

[1] Department of Mechanical Engineering, Tsinghua University, Beijing 100084, China

[2] Beijing Institute of Electronic System Engineering, Beijing 100854, China

[3] Beijing Key Lab of Precision/Ultra-precision Manufacturing Equipments and Control, Beijing 100084, China

Keywords Subsurface damage · Cutting force · Rotary ultrasonic machining · Optical glass

1 Introduction

Optical K9 glass is an outstanding functional brittle material, which has been widely used in various fields such as optics, electronics, thermodynamics, and fluidics [1]. However, owing to its inherent shortcomings such as high hardness, high strength, and low fracture toughness, K9 glass has become one of the most hard-to-machine materials, especially for the high quality requirement [2]. The machining of optical glass has attracted the attention of many researchers, aiming to improve efficiency and reduce cost [3]. To date, several investigations have been made using traditional methods for optical glass machining, which include cutting [4], grinding [5], milling [6], and lapping [7].

Rotary ultrasonic machining (RUM) is a nontraditional machining process, which combines the material removal mechanisms of diamond grinding and ultrasonic machining [8]. A rotating tool with metal-bonded diamond abrasives is ultrasonically vibrated in the axial direction [9]. At the same time, it feeds towards the workpiece at a constant feed rate [10]. The machining processes are rotary ultrasonic drilling (RUD), when the tool feed direction is parallel to the direction of ultrasonic vibration, and milling [rotary ultrasonic face machining (RUFM) as shown in Fig. 1, when the tool feed direction is perpendicular to the direction of ultrasonic vibration [11]. Compared with other machining methods applied in hard and brittle materials, RUM can obtain a lower cutting force, higher surface quality, and higher material removal rate [12]. However, most investigations reviewed in the literature concentrate on RUD. In addition, RUD has already been applied successfully to machine many types of materials, especially

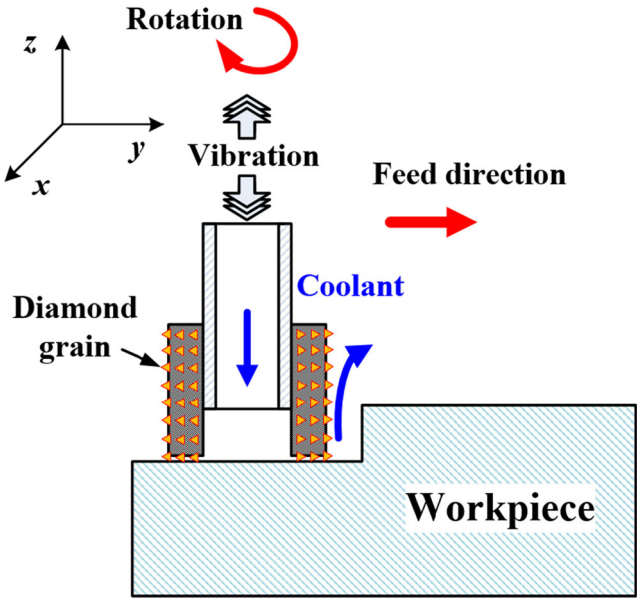

Fig. 1 Illustration of RUFM

for hard-to machine materials such as optical glass [13], advanced ceramic [14], titanium [15], and fiber-reinforced polymer composite [16]. Nevertheless, some studies have found RUFM to be workable for the machining of brittle material including optical K9 glass [17].

Any type of mechanical machining including RUFM would induce subsurface damage (SSD) in the machined surface of brittle material [18]. The SSD, which refers to a residual fractured crack on the top surface, considerably influences operational life, secular stability, and laser-induced damage threshold of optical elements [19, 20]. Diminishing or eliminating SSD by optimizing the process parameters or developing new machining methods has been investigated both experimentally and theoretically [21]. However, this optimization is founded on the accurate inspection or even prediction of the SSD depth. To date, a vast number of destructive and nondestructive techniques have been explored for the evaluation of SSD depth [22]. Typical nondestructive techniques consist of ultrasonic scanning microscopy, laser scattering, X-ray diffraction method, and total internal reflection microscopy [23, 24]. However, the accuracy of nondestructive techniques is unsatisfactory, whose results sometimes only provide qualitative data that restricts the correct determination of process parameters in a subsequent procedure. In addition, a relatively large safety factor must be used to guarantee the reliability of evaluation results at the expense of processing efficiency. Conversely, destructive evaluation techniques such as polishing have a believable accuracy by exposing the structure below the final surface without introducing new observable SSD. Typical destructive techniques include the chemical etching method, taper polishing, ball dimpling, a magnetorheological finishing (MRF) wedge, and MRF sporting [25, 26]. However, it is evidently undesirable for expensive components due to the inevitable effect of destructive evaluation techniques on the finished surfaces of the specimens. Another shortcoming of these destructive methods is that measuring efficiency is inadequate. Consequently, it has important theoretical significances and application prospects to develop a rapid and efficient method for evaluating the SSD depth of brittle material in RUFM.

In the RUFM of optical material, surface roughness and cutting force are much easier to evaluate than SSD [27]. Several investigations have been made to establish the relationship between surface roughness and SSD [27–29]. Lv et al. developed a nonlinear theoretical model to predict SSD depth by successfully measuring surface roughness in the RUFM of optical BK7 glass [30]. However, this method cannot be used to detect SSD depth during the RUFM of brittle material in real time. In contrast, the cutting force can be measured in real time. Therefore, it is beneficial if SSD depth can be predicted by measuring the cutting force. However, there is no model for the relationship between the cutting force and SSD depth in the RUFM of brittle material.

In this study, a mathematical model is developed to predict SSD depth by measuring the cutting force in the RUFM of optical K9 glass according to the brittle fracture mechanism of material removal. A series of experiments were performed to verify the theoretical model. Details of the methods are given in the following sections.

2 Development of predictive model for subsurface damage

For the development of a SSD model, some major assumptions and simplifications are used in this study.

1. Optical K9 glass is an ideally brittle material. The material is removed in brittle fracture mode on the workpiece surface.
2. All of the effective diamond grit taking part in the cutting process are rigid octahedrons like a Vickers indenter and have the same size and height.

2.1 Forming mechanism of subsurface damage of brittle materials in RUFM

The SSD depth is the main parameter to characterize SSD degree. For the time being, there are three kinds of methods for calculating SSD depth, namely clustering depth method, maximum depth method, and crack-distribution-density method [22]. The clustering depth method is usually applied to characterize the depth of a concentrated subsurface crack. The obtained results

using this method are relatively conservative. Thus, the clustering depth method is mainly used in such cases, as few requirements on the optical properties of the machined surface are required. Conversely, the maximum depth method can entirely characterize the depth of a subsurface crack induced by mechanical machining. In addition, if the subsurface crack of that depth is eliminated by polishing, purposes requiring ultra-precision of the machined surface can be achieved. The maximum depth method is employed in this research.

As mentioned in Section 1, diamond particles sintered on the end face of a tool ultrasonically impact and scratch the workpiece surface during diamond tool processing of brittle materials. Research has shown that the behavior of diamond particles acting on the workpiece surface can be equivalent to an indentation fracture with sharp indenters [31]. There are two material removal modes in the machining of hard and brittle materials, namely brittle fracture mode and ductile mode [32]. The ductile mode may be dominant when the cutting depth is relatively small. However, existing reports have shown that brittle fracture mode is the major material removal mode in the RUFM of brittle materials [11].

Median-radial and lateral cracks are generated, while diamond particles are indented into the workpiece surface. The two crack types have different effects. The chipping of a workpiece is primarily caused by the initiation and propagation of lateral cracks, which lead to material removal in brittle mode. In addition, surface roughness is determined by the propagation of lateral cracks. However, the median-radial cracks considerably influence the SSD of a machined surface. This conclusion has been employed in the investigation on material removal mechanisms and SSD characteristics in the grinding of optical material [33]. Zhang and Lv argued that in the RUFM of optical glass, the material removal characteristics are suitable to the indentation fracture mechanics of brittle material [11, 30].

The analysis on material removal characteristics in RUFM indicates that the material is removed under the combined action of abrasive grinding and ultrasonic impact. Thus, the SSD characteristic in the RUFM of optical glass depends on the load-carrying characteristics of diamond grit. According to indentation fracture mechanics, the model for the crack system of brittle material caused by the indentation with a sharp indenter is shown in Fig. 2, where F_n is the maximum impact force acting on the workpiece for one diamond particle, ψ is the semi-angle between two opposite edges of an abrasive particle, δ is the maximum penetration depth of a single abrasive particle penetrating into the workpiece, and C_m is the depth of the median crack from the unprocessed surface.

From the above analysis, we can conclude that the magnitude of C_m determines the SSD characteristic in the RUFM of optical glass.

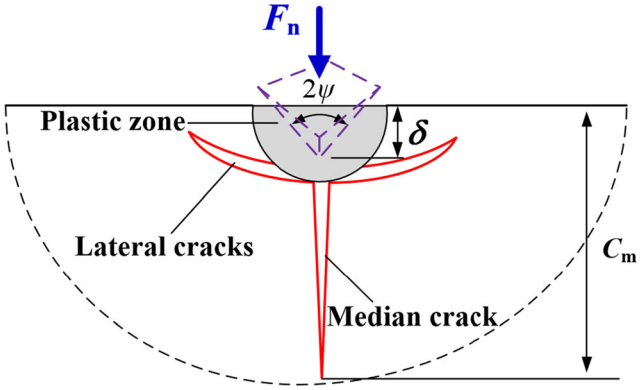

Fig. 2 Schematic diagram of the crack systems induced by a sharp indenter

Based on indentation fracture mechanics, Lambropoulos et al. developed the calculation formula of C_m as follows [29]:

$$C_m = {\alpha_k}^{2/3}\left(\frac{E}{H_v}\right)^{(1-q)2/3}(\cot\psi)^{4/9}\left(\frac{F_n}{K_{IC}}\right)^{2/3} \quad (1)$$

where E, H_v, and K_{IC} are the elastic modulus, microhardness, and fracture toughness, respectively; q is a dimensionless coefficient of correction (the value of 0.5 is used in this study); and α_k=0.027+0.090(q−1/3).

2.2 Relationships between measured cutting force and maximum impact force

Equation (1) builds the relationship between the maximum impact force and the depth of a subsurface medial crack. However, the exact instant cutting/impact force varies in a high-frequency cycle (about 20 kHz) during the RUFM of optical glass; meanwhile, the natural frequency of a typical dynamometer such as the Kistler 9256C2 (whose natural frequency is about 4.5 kHz) is much less than the ultrasonic frequency. Thus, the maximum impact force cannot be measured. In addition, the cutting force measured is an average force, with respect to time, of the actual impacting force acting on the workpiece surface. To model the relationship between SSD depth and measured cutting force, we must establish the correlation between the maximum impact force and measured cutting force. This work was done as follows.

In RUFM, the motions of diamond particles are considered to be sinusoidal due to their oscillatory nature. As shown in Fig. 3, the diamond abrasive particle on the end face of the diamond tool is not in continuous contact with the workpiece. The effective cutting time (Δt), which is the certain period of time that the diamond particle effectively processes the workpiece

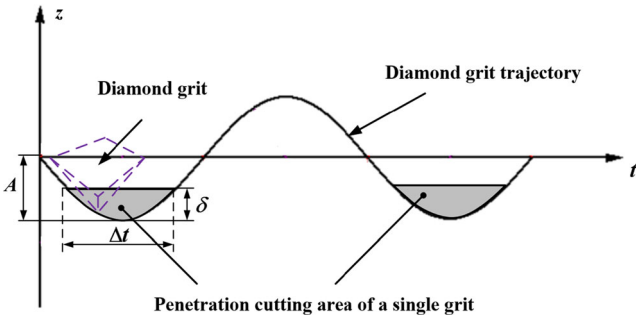

Fig. 3 Kinematic characteristics of the diamond particle in RUFM

surface in a single ultrasonic vibration cycle, can be calculated as

$$\Delta t = \frac{1}{\pi f}\arccos\left(1-\frac{\delta}{A}\right) \tag{2}$$

where A is the ultrasonic vibration amplitude and f is the ultrasonic vibration frequency.

According to the indentation fracture mechanics mechanism, the maximum impact force can be calculated [11] as

$$F_{\mathrm{n}} = \frac{1}{2}\xi\delta^2\tan^2\psi H_v \tag{3}$$

where ξ is the geometrical factor of the indenter.

Meanwhile, F_{n} can then be obtained as

$$F_{\mathrm{n}} = \frac{F_{\mathrm{m}}}{m} \tag{4}$$

where F_{m} is the maximum impact force between the diamond tool and the workpiece and m is the effective number of diamond particles taking part in the cutting.

Based on the knowledge on system dynamics, we get [16]

$$\int_T F_{\mathrm{m}}dt = \frac{F_{\mathrm{c}}}{f} \tag{5}$$

where F_{c} is the cutting force measured in the RUFM of optical glass.

The left part of Eq. (4) can be calculated as

$$\int_T F_{\mathrm{m}}dt = \lambda F_{\mathrm{m}}\Delta t \tag{6}$$

where λ is the coefficient of correction depending on the wave profile of actual impact force on the workpiece surface. For example, λ should be defined as 1, 0.5, or $2/\pi$ when the wave profile of the actual impact force is square [31], triangular [34], or sinusoidal [35], respectively.

Substituting Eqs. (5) and (6) into Eq. (4), the relationship between F_{c} and F_{n} is derived as

$$F_{\mathrm{c}} = \lambda{\cdot}m{\cdot}f{\cdot}F_{\mathrm{n}}{\cdot}\Delta t \tag{7}$$

2.3 Predictive model for subsurface damage

To simplify numerical computation, we simplify the equation for the contact time (Δt). There are two types of method to achieve this. One widely used in the literature [12, 36] is

$$\Delta t \approx \frac{\delta}{2Af} \tag{8}$$

Herein, we propose one that applies the principle of infinitesimal equivalence as

$$\Delta t \approx \frac{\sqrt{2}}{\pi f}\left(\frac{\delta}{A}\right)^{\frac{1}{2}} \tag{9}$$

Equations (2), (8), and (9) are depicted in Fig. 4. The figure illustrates that the simplifying precision of Eqs. (8) and (9) is strongly determined by the magnitude of δ/A. When δ/A is less than ~0.8, Eq. (9) has a higher simplifying precision than Eq. (8). Conversely, when δ/A is more than ~0.8, Eq. (8) has a higher simplifying precision than Eq. (9). Both simplifying

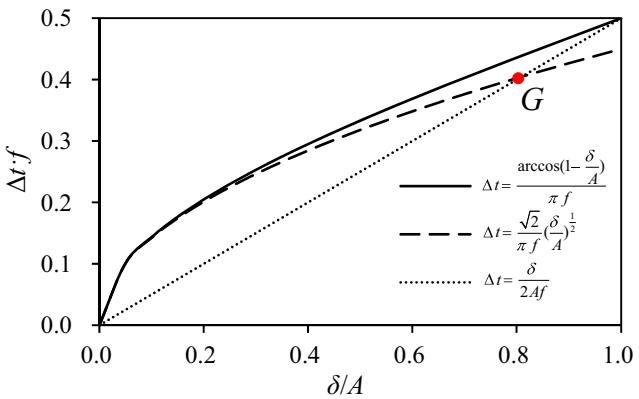

Fig. 4 Simplifying method of the equation for contact time (Δt)

methods are employed in the present paper to develop the predictive model for subsurface damage.

When Eq. (8) is employed, substituting Eq. (8) into Eq. (7), the relationship between F_c and F_n can be derived as

$$F_c = \frac{\lambda m F_n}{2A} \cdot \delta \tag{10}$$

Meanwhile, δ can be calculated from Eq. (3) as

$$\delta = \left[\frac{2F_n}{\xi \tan^2\psi H_v}\right]^{\frac{1}{2}} \tag{11}$$

Substituting Eq. (11) into Eq. (10), F_n can be expressed as the function of F_c

$$F_n = \left[\frac{A}{\lambda m}\right]^{\frac{2}{3}} \cdot [\xi H_v]^{\frac{1}{3}} \cdot [\tan\psi F_c]^{\frac{2}{3}} \tag{12}$$

Substituting Eq. (12) into Eq. (1), the relationship between the subsurface medial crack depth (C_m) and the measured cutting force (F_c) can be derived as

$$C_m = \frac{{\alpha_k}^{2/3} E^{1/3} A^{4/9} \xi^{2/9}}{H_v^{1/9} {K_{IC}}^{2/3} \lambda^{4/9} m^{4/9}} \cdot {F_c}^{\frac{4}{9}} \tag{13}$$

Taking the same approach, when Eq. (9) is employed, the relationship between the subsurface medial crack depth (C_m) and the measured cutting force (F_c) can be derived as

$$C_m = \frac{{\alpha_k}^{2/3} E^{1/3} (\cot\psi)^{8/45} A^{4/15} \xi^{2/15}}{2^{2/5} H_v^{1/5} {K_{IC}}^{2/3} \lambda^{8/15} m^{8/15}} \cdot {F_c}^{\frac{8}{15}} \tag{14}$$

Due to the distinct simplifying precision of Eqs. (8) and (9), we can summarize from Eqs. (13) and (14) that the SSD depth is a power function of the measured cutting force. The relationship between SSD depth and measured cutting force can be expressed as

$$d_{SSD} = \gamma {F_c}^{\chi} \tag{15}$$

where d_{SSD} is the predictive SSD depth, γ is the proportionality factor, and χ is the index of power function. In addition, the index χ is supposed to be the average value of $\frac{4}{9}$ and $\frac{8}{15}$ in consideration of the limited simplifying precision, namely χ=0.49.

3 Experimental procedure

3.1 Experimental apparatus and materials

Rotary ultrasonic face milling experiments were performed on Sauer Ultrasonic 50 (DMG, Bielefeld, Germany), which consists of an ultrasonic spindle system, a numerical control machining system, and a coolant system. The ultrasonic spindle system comprises of an ultrasonic spindle and a power supply. The power supply converts 50 Hz electrical supply to high-frequency (around 20 kHz) AC output. The piezoelectric transducer located in the ultrasonic spindle converts the electrical input into mechanical vibrations with ultrasonic frequency. The maximum ultrasonic machining spindle speed is 8000 rpm, and the maximum power of the rotary ultrasonic machine is 300 W. In the present study, an electroplated diamond hollow tool was used whose outer diameter is 10 mm, wall thickness is 1 mm, and diamond particle size (mesh) is D91. Processing fluid was used as internal and external coolants in the experiment, supplied by Blaser (Switzerland).

A fixture was mounted on a dynamometer attached to the machine table to hold the specimen. The piezoelectric dynamometer (9256C2) used in this study to record the cutting forces along the normal direction during the experiments was provided by Kistler Instrument Corp. The electrical signals from the dynamometer were amplified by an amplifier (5070A) and were then fed to a data recorder (2855A4). Then, the recorded data were displayed and saved on the computer with the help of DynoWare, which is professional software provided by Kistler. The sampling frequency was 5 kHz.

The workpiece material was K9 glass. Mechanical properties of the workpiece material obtained by indentation experiment are listed in Table 1.

3.2 Machining procedure

To verify the predictive model for SSD in RUFM developed in Section 2, experiments were conducted to obtain sufficient data concerning the SSD depth and measured cutting force. The design of experiments is given in Table 2. The experiments consist of three groups of input variables: spindle speed, feed rate, and cutting depth. The ultrasonic frequency was set at 17 kHz, which is the resonance frequency for the selected diamond cutter with the ultrasonic spindle. The ultrasonic

Table 1 Material properties of optical K9 glass

Density, ρ (g/cm^3)	2.5
Young's modulus, E (GPa)	85.9
Poisson's ratio, ν	0.28
Vickers hardness, H (GPa)	7.2
Fracture toughness, K_c (MPam$^{1/2}$)	0.8

Table 2 Machining variables and their values used in the experiment in the RUFM of optical glass

Experiment	Spindle speed (rpm)	Feed rate (mm/min)	Depth of cut (μm)	Cutting width (mm)
1st group	1000, 2000, 3000, 4000, 5000, 6000, 8000	6	60	10
2nd group	3000	2, 6, 8, 12, 16, 24	60	10
3rd group	3000	6	10, 20, 30, 60, 80, 120	10

amplitude of the diamond cutter was 15 μm as measured with a laser fiber vibrometer (Polytec, Germany), and the ultrasonic power was 13 W. The same diamond cutter was used during all experiments.

Experiments were also conducted to investigate the feasibility of RUFM of optical K9 glass by comparing it with the conventional grinding (CG) method. The machining variables and their values used in the experiment in CG of optical glass were the same as those used in the first and second group of RUFM, except that the ultrasonic supply was shut down.

3.3 Post-machining evaluation

In this study, the MRF technique that is suitable for SSD measurement of a slightly damaged sample was used to measure SSD depth. The MRF equipment (KDMRF-100) used in this study was provided by the National University of Defense Technology. First, to reveal a subsurface crack, the sample surfaces were placed in the etchant solution (2 % HF) for sufficient time duration. Afterwards, the method of ultrasonic cleaning was used to clean the sample surface. Then, the sample surfaces were polished with a sloped depression through the SSD layer. After that, a surface profilometer (Taylor Hobson Corp., Britain) was used to measure the depth profiles of the centerline of the MRF spots. Subsequently, the sample surfaces were placed on an inching platform after being cleaned with ethyl alcohol. An optical microscope STM6 (Olympus, Japan) was employed to observe the SSD morphology as well as to identify SSD depth. The SSD depth was determined by calculating the horizontal distance of the last cracks obtained from the inching platform to the depth profile obtained from the profilometer.

4 Results and discussion

4.1 Morphology of subsurface damage in RUFM

Figure 5 shows the typical SSD micrographs of K9 glass processed by RUFM. As shown in the figure, there are two types of SSD: one is the conchoidal morphology due to the lateral cracks and the other is the subsurface crack induced by a median-radial crack. The SSD distributed more intensively near the machined surface. In addition, the distribution density of the SSD decreases with the increase of depth. In this specimen, when the polishing depth is 1.8 or 3.2 μm, massive cracks with large size distribute around the machined surface. When the polishing depth is 6.9 μm, little and slight cracks

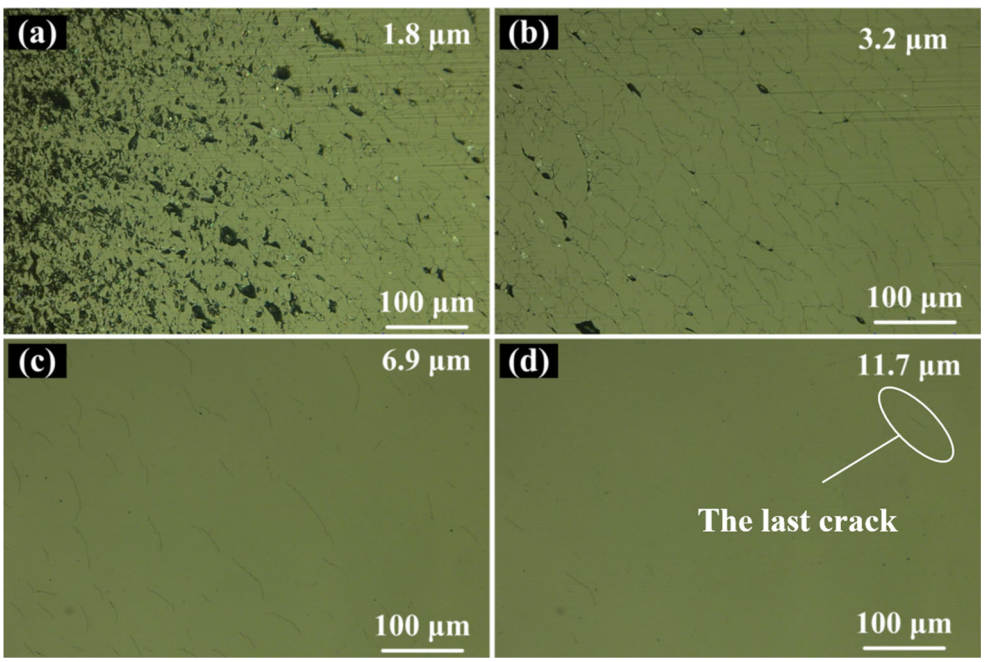

Fig. 5 **a**–**d** Typical SSD micrographs generated during RUFM

can be found under the machine surface. Otherwise, when the polishing depth is above 11.7 μm, the SSD vanishes completely and only undamaged substrate remains, which means that the SSD depth is 11.7 μm. Subsequently, this approach was used in the investigation of the relationship between SSD depth and measured cutting force.

4.2 Effect of process parameters on the subsurface damage

Figure 6 reflects the influence of processing parameter on the measured cutting force and SSD depth in RUFM and CG of optical glass, respectively. As shown in Fig. 6, the measured cutting force decreases with an increase of spindle speed; however, it increases as the feed rate increases in both RUFM and CG. Otherwise, under the same processing condition, the measured cutting force in RUFM is much smaller than that in CG. We can draw a conclusion that the RUFM method for machining of optical glass can reduce the measured cutting force by 30–50 %. Meanwhile, the variation tendency of the SSD depth with an increase in processing parameter (spindle speed and feed rate) is in accordance with that of the measured cutting force.

Generally, polishing is supposed to be a beneficial method for deducing the SSD depth of optical material, though inefficient due to its shearing mechanism of material removal.

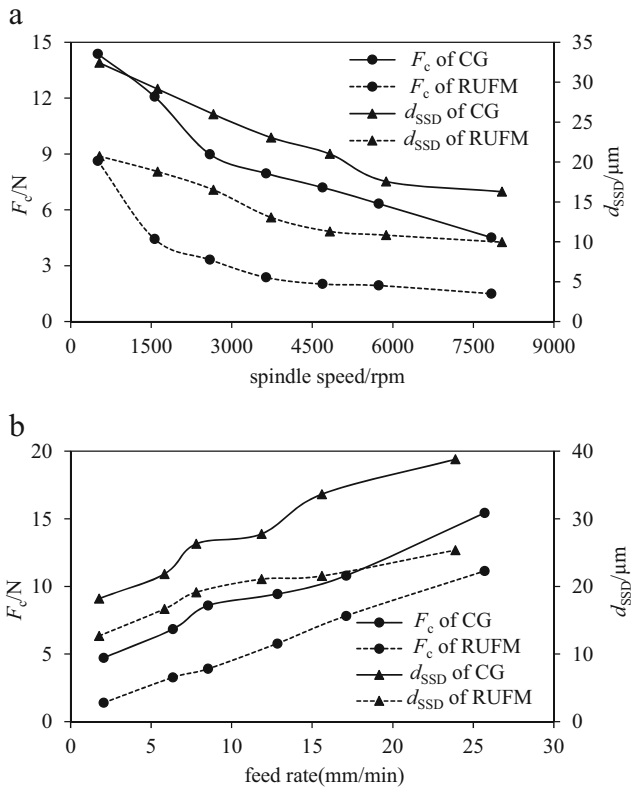

Fig. 6 **a**, **b** Effect of process parameters on the subsurface damage

Taking the MRF polishing of optical glass as an example, it would cost about 6 h to polish a specimen with a size of 100 mm×100 mm and a depth of 2 μm. Therefore, it can be concluded from the experimental results that RUFM is a desirable method for the precision machining of optical glass. For the optical element applied in ordinary circumstances where the element surface need not be polished, RUFM can improve its performance and stability with diminished SSD. Otherwise, for an ultra-precise optical element that needs to be polished, RUFM can reduce time and expense by diminishing the polishing depth. Thus, the cost of time and money can be economized by the employment of RUFM in the manufacturing of optical glass.

4.3 Verification of predictive model for subsurface damage

Figure 7 presents the relationship between measured cutting force and SSD depth in the RUFM of optical glass using a log–log coordinate. Using a linear fitting method, a regression equation (correlation coefficient is 0.9759) of log d_{SSD}–log F_c can be obtained

$$\log d_{SSD} = 0.48 \log F_c + 0.96 \tag{16}$$

Then, the power function can be derived as

$$d_{SSD} = 9.13 F_c^{0.48} \tag{17}$$

Comparing Eq. (17) with Eq. (15), we can obtain the magnitude of index (χ), χ=0.48, which is fairly close to the value of 0.49 applied in the predictive model. Therefore, the SSD model was well verified by the experiments.

It can be concluded that the developed predictive model for SSD can be applied to evaluate actual SSD depth by measuring the cutting force in the RUFM of optical glass. This is beneficial to the rapid and nondestructive detection of SSD in RUFM, providing a potential reduction of testing time and manufacturing cost.

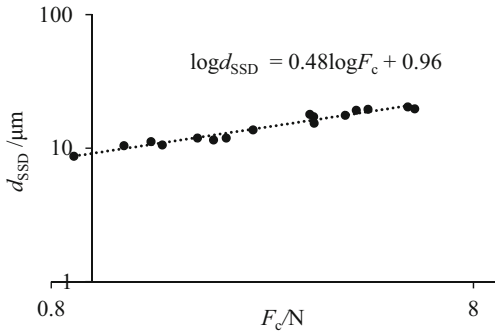

Fig. 7 Verification of the predictive model for subsurface damage

5 Conclusions

A predictive model for detecting the SSD depth was developed for RUFM of optical glass by measuring the cutting force for the first time. The relationship between measured cutting force and SSD depth was established by applying indentation fracture mechanics. The developed predictive model was experimentally verified in pilot experiments. Using this model, the depth of SSD was predicted rapidly and precisely in the RUFM of optical glass even in real time. The model showed that the subsurface damage depth was directly proportional to the exponent of measured cutting force (namely $d_{SSD}=\gamma F_c^{\chi}$). Meanwhile, the cutting force and SSD depth were compared between RUFM and CG, indicating that RUFM is a beneficial manufacturing method for optical glass with reduced cutting force and SSD depth. In addition, the predictive model of SSD depth can be used for other brittle materials in RUFM.

Acknowledgments We gratefully acknowledge the financial support for this research from the Beijing Natural Science Foundation (Grant No. 3141001), the Beijing Science and Technology Program (Grant No. D131100002713003), and the Funding of State Key Lab of Tribology (Grant No. SKLT2013B03).

Conflict of interest The authors declare that they have no competing interests.

References

1. Choi JP, Jeon BH, Kim BH (2007) Chemical-assisted ultrasonic machining of glass. J Mater Process Technol 191(1–3):153–156. doi:10.1016/j.jmatprotec.2007.03.017
2. Zhao CY, Gong H, Fang FZ (2013) Experimental study on the cutting force difference between rotary ultrasonic machining and conventional diamond grinding of K9 glass. Mach Sci Technol 17(1):129–144. doi:10.1007/s00170-014-6216-6
3. Gu WB, Yao ZQ, Liang XG (2011) Material removal of optical glass BK7 during single and double scratch tests. Wear 270(3–4): 241–246. doi:10.1016/j.wear.2010.10.064
4. Fang FZ, Chen LJ (2000) Ultra-precision cutting for ZKN7 glass. CIRP Ann Manuf Technol 49(1):17–20. doi:10.1016/S0007-8506(07)62887-X
5. Gu WB, Yao ZQ, Li HL (2011) Investigation of grinding modes in horizontal surface grinding of optical glass BK7. J Mater Process Technol 211(10):1629–1636. doi:10.1016/j.jmatprotec.2011.05.006
6. Arif M, Rahman M, San WY (2011) Analytical model to determine the critical feed per edge for ductile-brittle transition in milling process of brittle materials. Int J Mach Tools Manuf 51(3):170–181. doi:10.1016/j.ijmachtools.2010.12.003
7. Belkhir N, Bouzid D, Herold V (2009) Surface behavior during abrasive grain action in the glass lapping process. Appl Surf Sci 255(18):7951–7958. doi:10.1016/j.apsusc.2009.04.178
8. Kumar J (2013) Ultrasonic machining—a comprehensive review. Mach Sci Technol 17(3):325–379. doi:10.1080/10910344.2013.806093
9. Cong WL, Pei ZJ, Feng Q, Deines TW, Treadwell C (2012) Rotary ultrasonic machining of CFRP: a comparison with twist drilling. J Reinf Plast Compos 31(5):313–321. doi:10.1177/0731684411427419
10. Li ZC, Cai LW, Pei ZJ (2006) Edge-chipping reduction in rotary ultrasonic machining of ceramics: finite element analysis and experimental verification. Int J Mach Tools Manuf 46(12–13):1469–1477. doi:10.1016/j.ijmachtools.2005.09.002
11. Zhang CL, Zhang JF, Feng PF (2013) Mathematical model for cutting force in rotary ultrasonic face milling of brittle materials. Int J Adv Manuf Technol 69(1–4):161–170. doi:10.1007/s00170-013-5004-z
12. Pei ZJ, Prabhakar D, Ferreira PM, Haselkorn M (1995) A mechanistic approach to the prediction of material removal rates in rotary ultrasonic machining. J Manuf Sci Eng 117(2):142–151. doi:10.1115/1.2803288
13. Zhang CL, Feng PF, Wu ZJ, Yu DW (2011) An experimental study on processing performance of rotary ultrasonic drilling of K9 glass. Adv Mater Res 230–232:221–225. doi:10.4028/www.scientific.net/AMR.230-232.221
14. Li ZC, Jiao Y, Deines TW, Pei ZJ (2005) Rotary ultrasonic machining of ceramic matrix composites: feasibility study and designed experiments. Int J Mach Tools Manuf 45(12–3):1402–1411. doi:10.1016/j.ijmachtools.2005.01.034
15. Churi NJ, Pei ZJ, Treadwell C (2007) Rotary ultrasonic machining of titanium alloy (Ti-6Al-4V): effects of tool variables. Int J Precis Eng 1(1):85–96
16. Cong WL, Pei ZJ, Sun X, Zhang CL (2014) Rotary ultrasonic machining of CFRP: a mechanistic predictive model for cutting force. Ultrasonics 54(2):663–675. doi:10.1016/j.ultras.2013.09.005
17. Zhang CL, Cong WL, Feng PF, Pei ZJ (2013) Rotary ultrasonic machining of optical K9 glass using compressed air as coolant: a feasibility study. Proc Inst Mech Eng B J Eng 228(4):504–514. doi:10.1177/095440541350 6195
18. Agarwal S, Rao PV (2008) Experimental investigation of surface/subsurface damage formation and material removal mechanisms in SiC grinding. Int J Mach Tools Manuf 48(6):698–710. doi:10.1016/j.ijmachtools.2007.10.013
19. Miller PE, Suratwala TI, Wong LL, Feit MD (2005) The distribution of subsurface damage in fused silica. Proc SPIE 5991:1–25. doi:10.1117/12.638821
20. Wang J, Li Y (2011) Evaluating subsurface damage in optical glasses. J Eur Opt Soc Rapid 6:11001
21. Wang Z, Wu Y, Dai YF, Li SY (2008) Subsurface damage distribution in the lapping process. Appl Opt 47(10):1417–1426. doi:10.1364/AO.47.001417
22. Wang Z (2008) Study on the detection and control techniques of subsurface damage in optical fabrication. Ph. D. thesis, National University of Defense Technology
23. Ellingson JA, Todd JA, Sun J (2001) Optical method and apparatus for detection of defects and microstructural changes in ceramics and ceramic coatings. US Patent 6285449:B1
24. Meeder M, Mauret T, Booij S, Braat J, Fahnle O (2003) Optimization of polishing processes by using iTIRM for in-situ monitoring of surface quality. Proc SPIE 5180:40–46. doi:10.1117/12.503679
25. Yoshikawa M, Zhang B, Tokura H (1987) Observations of ceramics surface cracks by newly proposed methods. J Ceram Soc Jpn 95: 961–969
26. Affatigato M, Osborne DH, Haglund RF (1996) Effect of surface roughness on the acid etching of amorphous silica. J Am Ceram Soc 79:688–694

27. Hed PP, Edwards DF (1987) Relationship between subsurface damage depth and surface roughness during grinding of optical glass with diamond tools. Appl Opt 26:2491
28. Neauport J, Ambard C, Cormont P, Darbois N, Destribats J, Luitot C, Rondeau O (2009) Subsurface damage measurement of ground fused silica parts by HF etching techniques. Opt Express 17:20448–20456
29. Lambropoulos JC, Jacobs SD, Ruckman J (1999) Material removal mechanisms from grinding to polishing. Ceram Trans 102:113–128
30. Lv DX, Huang YH, Tang YJ, Wang HX (2013) Relationship between subsurface damage and surface roughness of glass BK7 in rotary ultrasonic machining and conventional grinding processes. Int J Adv Manuf Technol 67(1–4):613–622. doi:10.1007/s00170-012-4509-1
31. Liu DF, Cong WL, Pei ZJ, Tang Y (2012) A cutting force model for rotary ultrasonic machining of brittle materials. Int J Mach Tools Manuf 52(1):77–84. doi:10.1016/j.ijmachtools.2011.09.006
32. Pei ZJ, Ferreira PM (1998) Modeling of ductile-mode material removal in rotary ultrasonic machining. Int J Adv Manuf Technol 38(10–11):1399–1418. doi:10.1016/S0890-6955(98)00007-8
33. Zarepour H, Yeo SH (2012) Predictive modeling of material removal modes in micro ultrasonic machining. Int J Mach Tools Manuf 62:13–23. doi:10.1016/j.ijmachtools.2012.06.005
34. Zhou XG (2011) Study on the machining mechanisms and surface quality in ultrasonic vibration grinding of silicon nitride ceramics. Master thesis, Harbin Institute of Technology
35. Astashev VK, Babitsky VI (2007) Ultrasonic processes and machines: dynamics, control and applications. Springer, Berlin, pp 208–209
36. Xiao X, Zheng K, Liao W (2014) Theoretical model for cutting force in rotary ultrasonic milling of dental zirconia ceramics. Int J Adv Manuf Technol 75(9–12):1263–1277. doi:10.1007/s00170-014-6216-6